J. Anat. (1995) 187, pp. 563–581, with 19 figures Printed in Great Britain

Cells and circuits contributing to functional properties in area V1 of macaque monkey cerebral cortex: bases for neuroanatomically realistic models

J. S. LUND[1], Q. WU[1], P. T. HADINGHAM[2] AND J. B. LEVITT[1]

[1] *Department of Visual Science, Institute of Ophthalmology, London, UK, and* [2] *Department of Computer Science, The University of Western Australia, Nedlands, WA 6907, Australia*

(*Accepted 15 August 1995*)

ABSTRACT

Anatomical and physiological data obtained from investigations of area V1 of the macaque monkey visual cerebral cortex have been used in 3 models outlining possible circuitry underlying functional properties of the region. The 3 models use, respectively, a fully implemented computer neural network, a mathematical formulation of interactions in a descriptive model of anatomical circuitry and a purely descriptive account of circuitry that could underlie particular functions. The 1st 2 models involve as part of their design an interpolation principle where afferents of opposite physiological property establish spatially offset but adjacent terminal fields and the postsynaptic neurons' dendrites have a continuum of different degrees of overlap into the 2 afferent pools and therefore different synaptic weights from the 2 afferents; this creates a functional and spatial gradient of response properties in the postsynaptic neurons between the properties of the different sets of afferents. The 3rd model examines lateral excitatory and inhibitory interactions in such gradients. Model 1 addresses the transformation of distinct thalamic axon properties to a gradient of response properties in postsynaptic spiny stellate neurons in layer 4C of V1. Model 2 proposes circuitry producing orientation specificity in V1 that begins by generating specificity of responses to orthogonal orientations; this is achieved by means of orthogonally oriented lateral axon projections made by the layer 4C spiny stellate neurons; this is followed by generation of a full cycle of orientation specificities by means of pyramidal neuron dendritic overlap across spatially separated fields of spiny stellate neuron axons responding preferentially to orthogonal orientations. Model 3 describes a circuitry to explain inhibitory and facilitatory interactions observed to occur in single unit responses when the classical receptive field is stimulated concurrently with the surround region. All the proposed models make predictions that can be tested by further anatomical and physiological experiments in the real visual cortex.

Key words: Contrast sensitivity; orientation specificity; centre-surround interaction; visual cortex; primates.

INTRODUCTION

A wealth of anatomical and physiological information has accumulated in recent years concerning the organisation of the primary visual cortex, area V1, of the macaque monkey. However, we are still without explanations for how key physiological properties of the region are generated. Modellers have in general used network architectures that have little resemblance to the real anatomical circuitry and often the models cannot be confirmed by new experiments in the real animal. There is an urgent need for models that are as biologically realistic as possible; they should lead to new experiments in the live animal that can confirm or modify the models proposals in regard to how anatomical circuitry and neuron properties may really underlie cortical function. The actual circuitry and physiological data are sufficiently complex that modelling should now be an essential tool in the biologist's laboratory helping to crystallise more precisely the logic behind new data collection and helping to steer biological experiments on cerebral cortex in productive directions. We would like to review here our current attempts at biologically

Correspondence to Professor J. S. Lund, Department of Visual Science, Institute of Ophthalmology, Bath Street, London EC1V 9EL, UK.

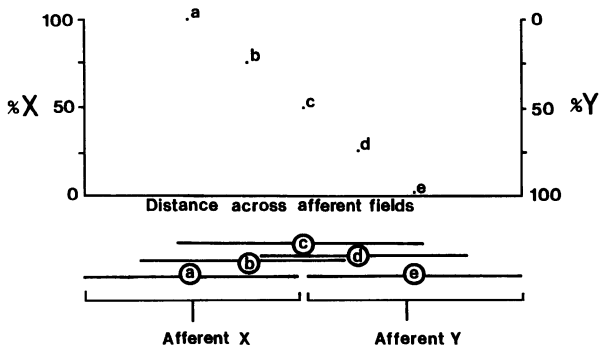

Fig. 1. Diagram showing the basic principle used in our models of parcellated afferent terminal territories (X and Y) with overlaid continuum of postsynaptic neuron (a–e) dendritic fields. Where a close spatial match is made between the size of the afferent terminal territories and the average dendritic field size of the postsynaptic neurons, a perfect functional gradient (plotted above) between the afferent properties can be achieved in the continuum of laterally offset postsynaptic neurons by simple spatial sampling from the 2 afferent populations according to the degree of overlap (and therefore synaptic weight) of the postsynaptic neuron dendrites into the 2 afferent pools.

realistic models for area V1 functional architecture with the suggestion that basic principles of the models proposed may be a useful framework for understanding general features of cortical organisation, not just those concerned with vision.

One key feature of the models we propose is that particular functional properties are presented to the cortical neuropil by afferents having spatially nonoverlapping but adjacent terminal zones; a continuum of dendritic overlap by the postsynaptic cortical neurons between the different afferent terminal zones then allows a functional gradient to be created in the response properties of the postsynaptic neurons depending on the relative weight of synapses from the 2 different afferent pools (Fig. 1). We can refer to the underlying computational idea of such models as an 'interpolation principle' since in mathematical terms the neural networks in such models accomplish interpolation of intermediate values from sets of extreme, and often orthogonal, values according to specific combination rules. In our models the afferents may be extrinsic thalamic fibre populations or intrinsic interlaminar projections. A close spatial match is required between the territory occupied by each afferent terminal pool and the average size of the dendritic fields of the individual postsynaptic neurons for this interpolation scheme to work. Real anatomical and physiological data are used as the bases for the models outlined below. Predictions regarding real but as yet unexplored features of anatomy and physiology, testable in further biological experiments, are an important outcome of the models.

Three models are discussed below which are currently being explored in some detail in our laboratory and are presented in summary form in this account to illustrate how anatomical features can be usefully included in the formulation of cortical models. The 1st model, which has been fully developed as a working computer simulation incorporating many aspects of the real connectional anatomy and appropriate physiological properties, addresses the very first step in the transfer of information from thalamic afferents to postsynaptic spiny stellate neurons, in V1 layer 4C. The primary visual thalamic nucleus, the dorsal lateral geniculate nucleus (dLGN), is divided into 2 clear divisions—the parvocellular (P) layers which receive input from beta ganglion cells in the retina and magnocellular (M) layers that receive input from alpha retinal ganglion cells. The cells of the M and P dLGN divisions retain the visual field properties of the alpha and beta retinal ganglion cells that project to them, the M cells having on average larger visual fields, higher contrast sensitivity and better temporal resolution, and the P cells having smaller visual fields, lower contrast sensitivity and responding to low as well as high temporal frequencies —and, unlike the M cells, often having chromatically opponent centre surround visual field organisation (Wiesel & Hubel, 1966; Hicks et al. 1983; Derrington & Lennie, 1984). Our 1st model proposes that there is a loss of the clear M and P channel segregation seen in the lateral geniculate nucleus (LGN) in layer 4C with replacement by a functional gradient between the M and P input properties in terms of contrast sensitivity and visual field size. The 2nd model proposes circuitry by which orientation specificity could be generated within layer 4C, first as a sparsely represented specificity to orthogonal orientations, then, from these orthogonals, the circuitry for generation of specificity to a complete cycle of orientations in the superficial layers. The 3rd model proposes an anatomical substrate for interactions observed between the classical receptive field and surround regions during single unit physiological recording from orientation specific neurons with V1.

MODEL 1: GENERATION OF A FUNCTIONAL GRADIENT FOR RECEPTIVE FIELD SIZE AND CONTRAST SENSITIVITY FROM PROPERTIES OFFERED BY MAGNOCELLULAR AND PARVOCELLULAR LATERAL GENICULATE INPUTS TO LAYER 4C OF AREA V1

Relays from the magnocellular (M) and parvocellular (P) divisions of the LGN of the thalamus are known to end in nonoverlapping terminal territories in the

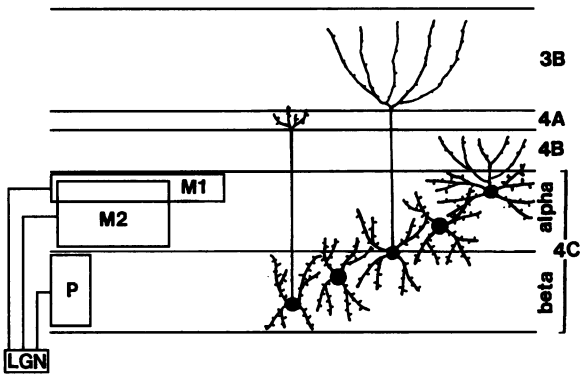

Fig. 2. Diagram of segregated territories of thalamic inputs from magnocellular (M) and parvocellular (P) layers of the LGN and overlap of dendrites of spiny stellate neurons in layer 4C. Three partially overlapped output channels arise from layer 4C; these are indicated as axons to layer 4A from layer 4C beta, output to interblob territories of layer 3B from mid layer 4C, and output to layer 4B from layer 4C alpha. Anatomical evidence is available (quoted in the text) for these features of organisation. We predict on the basis of both anatomical and physiological information quoted in the text that M1 input arises from a different type of magnocellular LGN neuron from the M2 magnocellular input.

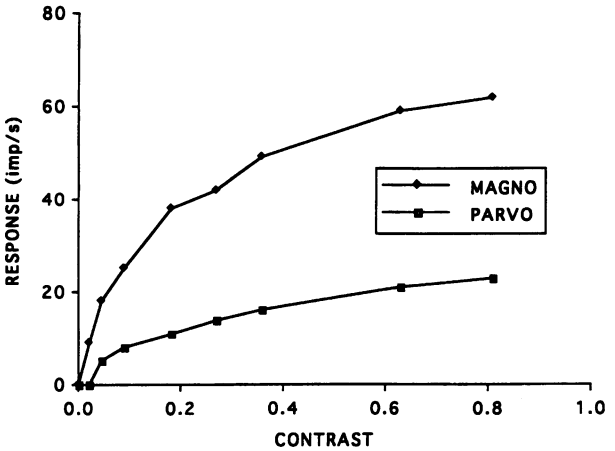

Fig. 3. Contrast response functions of a typical M and P cell in the LGN of the macaque monkey (adapted from Shapley, 1990).

alpha and beta subdivisions respectively of layer 4C (Fig. 2) in area V1 (Hubel & Wiesel, 1972). The thalamic axons terminate on spiny stellate neurons, believed to be the excitatory neurons of this layer where they provide a relatively small proportion, perhaps 6%, of the synapses on the stellate cell dendritic spines (Anderson et al. 1994; Peters et al. 1994). The dendritic fields of the spiny stellate neurons at different depths in the layer are of constant size and have a constant spine number in mature animals (Lund & Holbach, 1991). The dendrites of spiny stellate neurons in the middle depth of layer 4C lap freely over the border between the alpha and beta divisions extending into the terminal territories of both M and P axons. In an earlier study of the morphology of the incoming M axons (Blasdel & Lund, 1983), it was observed that while the individual arbors of the majority of M and all P axons extended the full depth of either the alpha or beta division, an infrequently labelled population of large M axons layered only along the upper half of the alpha division; these 2 M fibre distributions are labelled M1 and M2 in Figure 2. We will show that in our model we need to assign an especial importance to the input at the top of layer 4C and the question then arises what the nature of the M1 axons may be. It is known from physiological studies that the fastest conducting M axons are found to terminate in upper 4C alpha (Bullier & Henry, 1980) and in physiological recording in the LGN it has been found that neurons of Y type in the M layers receive the fastest conducting retinal ganglion cell input (Shapley et al. 1981). Since a fast conducting route would be especially valuable for motion perception, and inhibitory neurons making widespread lateral connections (a possible substrate underlying this function) lie at the top of layer 4C (Lund, 1987), we therefore propose that the M input to upper 4C alpha may arise from M fibres with larger fields and faster conduction velocities, possibly of Y type (Shapley et al. 1981) while another M fibre group, possibly of X type, terminates through the depth of the alpha division, i.e. partially overlapped with the MY input (see Fig. 2).

In the LGN, M and P cells differ markedly in their physiological properties such as contrast sensitivity and receptive field size. Figure 3 shows typical contrast response functions for M and P cells as adapted from Shapley (1990) and reveals that these 2 classes of cells have different maximum firing rates and contrast sensitivities (where contrast sensitivity is defined as the reciprocal of the contrast level to elicit a criterion response). It is also known that within the crossed or uncrossed optic pathways, at matched retinal eccentricities, LGN M cells have on average receptive fields with centre regions 2 to 3 times the diameter of the centre of P cells receptive fields (Derrington & Lennie, 1984) as mapped with achromatic sinusoidal gratings. In contrast to the LGN, layer 4C cells in V1 receiving the LGN input appear to show a gradient in receptive field size and contrast sensitivity through the depth of the 4C layer as illustrated in Figure 4 replotted from data shown by Blasdel & Fitzpatrick (1984) (Fig. 4*A*) and as a log plot from Hawken & Parker (1984) (Fig. 4*B*). The log plot of the data of Hawken & Parker (Fig. 4*B*) emphasises that the steep rate of change in function in upper 4C alpha seen in Figure 4*A* is not due to limited sampling problems.

An intriguing question involved in this transformation in properties from the LGN to layer 4C is how

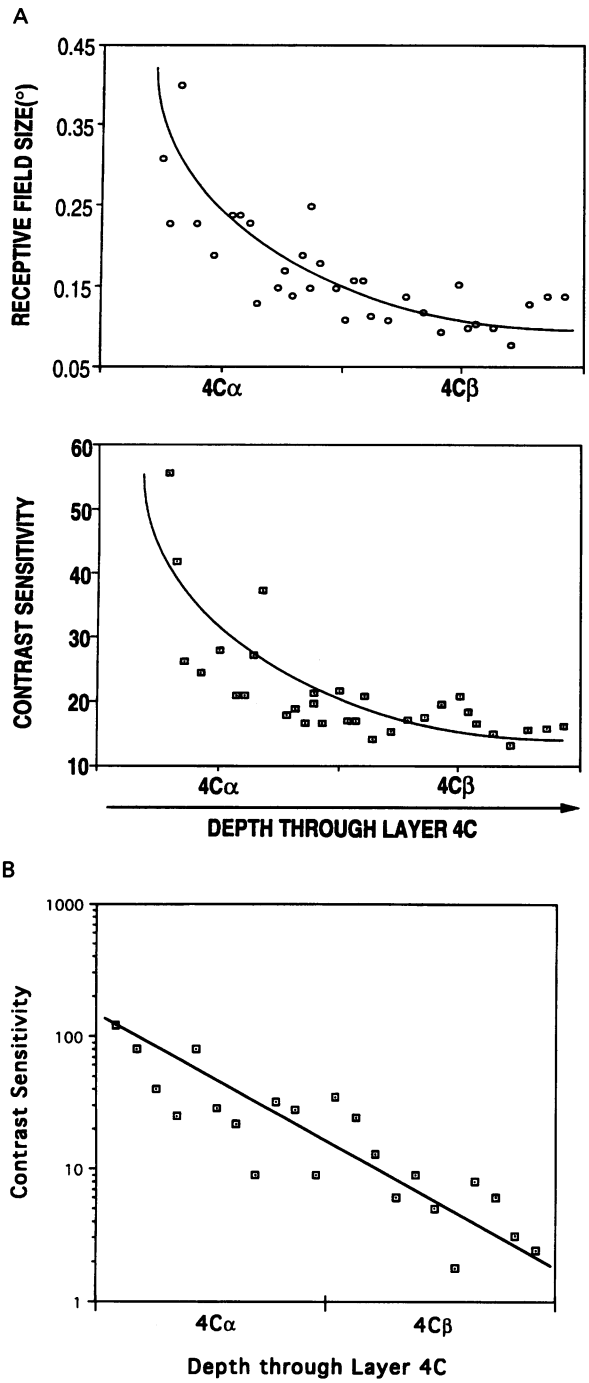

Fig. 4. (*A*) Two plots showing visual field size and contrast sensitivity respectively of cortical cells recorded through the depth of layer 4C (replotted from Blasdel & Fitzpatrick, 1984). Note that the receptive field size and contrast sensitivity changes gradually with depth in the layer. The solid line is the best fitting exponential function through these data points to illustrate their progressive change in properties. (*B*) Linear-logarithmic plot of contrast sensitivity measures for neurons encountered at different depths in layer 4C replotted from Hawken & Parker (1984).

the distinct sets of inputs from LGN are combined to create a functional gradient. Based on the anatomical organisation of layer 4C and the interpolation principle outlined above, we suggest that the functional gradient in layer 4C is determined in part by numerical weight of synapses from different types of thalamic input, which in turn is determined by the degree of dendritic overlap of the recorded cells into the M and P axon territories (see Fig. 2).

To explore this prediction more formally, we have built a computer neural network model for this transformation of physiological response properties between LGN and layer 4C spiny stellate neurons (Wu et al. 1994) using a simulation program which we have developed with the specific aim of building anatomically based network models. This model differs from many neural network models in that we do not allow the network to train its connections to the desired state but rather constrain the connections by using known anatomical and physiological data and hard-wire the connectivity. This connectivity is sufficiently complex that we could not predict the outcome of the model. The program currently runs on the Macintosh platform and was implemented in THINK-C Version 5.0. This simulation program has 2 prominent features as distinct from other neural network simulators. (1) It is very easy to define any network architecture and connectivity in the network according to anatomical data, either via a predefined file or through on-line interactive commands. (2) It provides a good graphic interface to facilitate visualisation of simulated anatomical connectivity as well as simulated physiological results. Apart from antagonistic centre-surround configuration for our retinal ganglion cell receptive fields, the model uses purely excitatory circuitry. The network architecture for our retina to layer 4C model is illustrated in Figure 5; the model consists of 1 input layer representing the retinal ganglion cell layer, 3 layers for the 3 divisions in the LGN (i.e. M1, M2, and P), and 8 layers representing various depths of layer 4C: 4 top layers for 4C alpha and 4 lower layers for 4C beta. The cell density for different layers and connectivity from retina to LGN and LGN to layer 4C are all constrained by anatomical findings as listed in the Table. An important parameter in any neural network model is the weights associated with the connections between the units. As mentioned earlier, it is known that spiny stellate cells in layer 4C each have a similar total number of spines on their dendrites (Lund & Holbach, 1991); we propose in addition, as an important element in the model, that each spiny stellate neuron may, as part of a constant total synaptic load, have a constant proportion of that load made by thalamic terminals, perhaps 6% of their total input (Anderson et al. 1994; Peters et al. 1994). This constant total synaptic weight

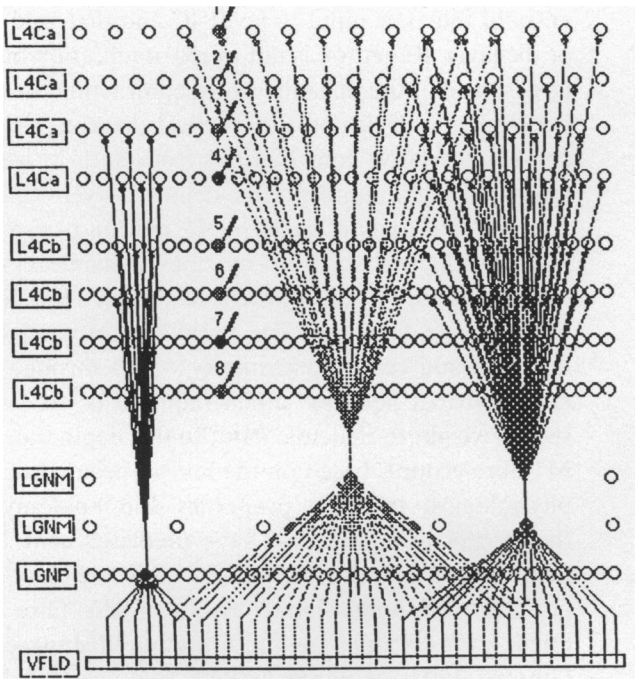

Weights distribution

4Cα		20	80
		42	58
	23	77	
	36	64	
4Cβ	50	50	
	80	20	
	100		
	100		
	P	M2	M1

Fig. 5. On the left is illustrated the network architecture of our model for geniculocortical transfer—as the transfer occurs in layer 4C, we also refer to it as a model for the functional architecture of layer 4C. The model consists of 1 input layer representing the retina or visual field (VFLD), 3 layers for the 3 divisions in the LGN (i.e. M1, M2, and P), and 8 layers representing various depths of layer 4C: 4 top layers for 4C alpha and 4 lower layers for 4C beta. The connectivity from the input layer to the LGN layers are constrained by relevant physiological findings such that the LGN cells have centre-surround organisation and that the centre size of the M cells are about 2 to 3 times larger than that of the P cells (Derrington & Lennie, 1984), as illustrated by the afferents convergent onto the LGN cells. The cell density for different layers in the LGN and layer 4C and the connectivity from LGN to layer 4C are all constrained by relevant anatomical findings as listed in the Table. The projections from the LGN cells making contacts with spiny stellate cells in layer 4C have different widths for M1, M2 and P axon arbors. To the right are listed the average weights for the 3 LGN afferent sets onto spiny stellae neurons at the 8 different depths in the simulated layer 4C when physiological output from layer 4C in the model (see Fig. 7) most closely matches the real physiological data (shown in Fig. 4).

Table. *Anatomical constraints used in the neural network for layer 4C in V1*

Numbers of LGN-P:LGN-M cells = 6:1 (O'Kusky & Colonnier, 1982)
Width of LGN-P:LGN-M2 axon fields = 1:6 (Blasdel & Lund, 1983)
Width of LGN-M2:LGN-M1 axon fields = 2:3 (unknown, but see Blasdel & Lund, 1983)
Numbers of LGN cells (P & M):4C(α & β) cells = 1:100 (Chow et al., 1950)
Numbers of 4Cα:4Cβ cells = 3:5 (O'Kusky & Colonnier, 1982)
Numbers of 4Cα:4Cβ spiny stellate neuron dendritic spines = 1:1 (Lund & Holbach, 1991)
Dendritic overlap for 4Cα and β cells (Lund, 1990)

per neuron is used as an important constraint for setting the weights from LGN to layer 4C neurons in our model. Thus, if the total input (IN) to each layer 4C cell is as follows:

$$\mathrm{IN} = \sum_i \mathrm{IN}_{\mathrm{P}}^i \bullet W_{\mathrm{P}}^i + \sum_i \mathrm{IN}_{\mathrm{M2}}^i \bullet W_{\mathrm{M2}}^i + \sum_i \mathrm{IN}_{\mathrm{M1}}^i \bullet W_{\mathrm{M1}}^i \quad (1)$$

(where $\mathrm{IN}_{\mathrm{P}}^i$, $\mathrm{IN}_{\mathrm{M2}}^i$, and $\mathrm{IN}_{\mathrm{M1}}^i$ are the inputs from the 3 LGN afferent sets as i goes through these input sets respectively, and W_{P}^i, W_{M2}^i, and W_{M1}^i are the connectional weights associated with each of these inputs, respectively) then the total weights for the 3 different LGN input sets

$$W_{\mathrm{P}} = \sum_i W_{\mathrm{P}}^i,\ W_{\mathrm{M2}} = \sum_i W_{\mathrm{M2}}^i \quad \text{and} \quad W_{\mathrm{M1}} = \sum_i W_{\mathrm{M1}}^i$$

satisfy the following constraint:

$$W_{\mathrm{P}} + W_{\mathrm{M2}} + W_{\mathrm{M1}} = \text{constant} \quad (2)$$

which represents the constraint that each cortical neuron in layer 4C has a constant synaptic load. The solid curves in Figure 6 replot the progression seen in

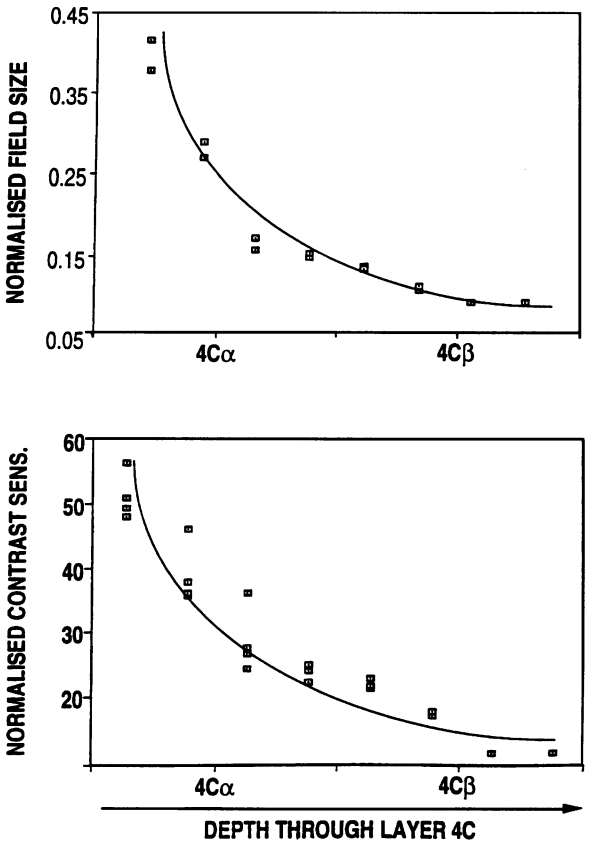

Fig. 6. Simulation results for receptive field size and contrast sensitivity obtained from units at different depths in layer 4C of the model with weights as shown in Figure 5. Lines are best fitted exponential functions. Slight variation between response properties of units at the same depth are due to slight variation in the local lateral overlap of the LGN axon arbors in the model.

Figure 4 relative to real physiological data. We used this progression to determine the best-fit weights for the 3 thalamic afferents on the layer 4C cells at 8 different levels in layer 4C (see Fig. 5); for these weights the simulated physiological results of receptive field size and contrast sensitivity from cortical cells in layer 4C in our model network as shown in Figure 6 closely match the actual results (here illustrated as the best fit curve) of recording through the depth of the layer (see Fig. 4). The best fit weights of different thalamic axon populations on cells at different depths listed in Figure 5 therefore represent our prediction for the actual synaptic weighting in vivo. The model is based on the assumption that under the conditions used by the physiologists for their recording experiments (Blasdel & Fitzpatrick, 1984; Hawken & Parker 1984) the layer 4C neurons each require the majority of their thalamic inputs to be active before they reach their firing point threshold.

Important conclusions from this model are that the segregation of M and P channels is lost at the first entry of thalamic input to layer 4C and that field size of the layer 4C neuron is not simply a reflection of the largest field of the thalamic axons contracting the cell, but that the field of the cortical neuron reflects combined relative contributions from both M and P inputs throughout most of the depth of layer 4C. The contrast sensitivity of the layer 4C neuron is also not just the highest offered by the thalamic axons converging on the cell but reflects a clear relation to the receptive field size. The rapid rate of change in field size and contrast sensitivity values through the upper part of layer 4C alpha required us to assign special weight to thalamic input to this depth (i.e. our M1 fibre group); based on the known peculiarities in physiological response properties and anatomy of thalamocortical fibres we have predicted that MY fibres could be the reason for this weight. The particular temporal characteristics of MY fibre and upper layer 4C alpha neuron firing rates (Maunsell & Gibson, 1992), a larger visual field size of MY compared with MX axons (as used in the model and based on the assumption that there are fewer MY (M1) than MX (M2) cells in the LGN and therefore each MY cell might be expected to have a larger visual field than individual MX cells); if MY fibres do not provide the answer to the rapid change in properties observed at the top of layer 4C alpha, it is possible that pooled visual fields by virtue of extensive lateral cross connections which are prominent in the anatomy of upper layer 4C alpha (Fitzpatrick et al. 1985; Yoshioka et al. 1994) could contribute to this increased weight; another feature that may enter into the response properties of neurons at the top of layer 4C is the apparent lack of inhibition from local circuit neurons shown to provide synapses to the cell bodies and dendrites of spiny stellate neurons deeper in the layer (interneuron type 4C beta and alpha type 1: Lund, 1987; Mates & Lund, 1983; or clutch cell: Kisvárday et al. 1986). This may allow a more rapid response and heightened firing rate in response to thalamic inputs in the upper 4C alpha neurons compared with those deeper in the layer. From our earlier studies of interneuron relays between different strata within 4C itself (Lund, 1987), and descending into mid layer 4C from layers above (Lund & Yoshioka, 1991) we would predict that activity in the 4C response gradient should be modifiable.

In summary, this model illustrates that it is likely to be the combined sum of activity from the thalamic inputs onto the cell that brings the layer 4C neuron to firing point, and that the response of the postsynaptic cell is not simply a direct reflection of just those thalamic axons with largest visual field or highest

contrast sensitivity that provide synaptic contacts to it.

MODEL 2: GENERATION OF ORIENTATION SPECIFICITY TO ORTHOGONAL ORIENTATIONS IN OFFSET NEURON SETS IN MIDLAYER 4C WITH SUBSEQUENT GENERATION OF A FULL RANGE OF ORIENTATION SPECIFICITIES IN LAYERS 3B AND UPPER 4C ALPHA

A variety of models have been proposed for generating orientation specificity (for a review, see Ferster & Koch, 1987), including that originally outlined by Hubel & Wiesel (1977) proposing convergence of thalamic axons from rows of LGN cells crossing the visual field at a variety of angles. While there is some evidence that this may occur in ferret layer 4 where most neurons are orientation specific (Chapman et al. 1991), in the monkey many neurons in thalamic recipient layer 4C lack orientation specificity and orientation specific neurons only become a significant part of the neuron population at the very top of the 4C layer. Recent observations in our own and other laboratories of lateral connections made by spiny stellate neurons within layer 4C have suggested to us (P. Hadingham et al. unpublished) that in the monkey oriented lateral connections made by the neurons postsynaptic to thalamic inputs could initiate orientation specificity. A very economical substrate, generating specificity to orthogonal orientations, could be used to generate a full range of orientation specific neurons as a gradient between these orthogonally tuned start points using an interpolation principle. There is a considerable weight of psychophysical data that shows vertical and horizontal axes to have an advantage over oblique orientations in visual discrimination tasks in the adult human (e.g. Jenkins, 1985). These same axes predominate numerically in the adult cat and monkey (Poggio & Fischer, 1977, Blakemore et al. 1981) in at least the foveal and parafoveal regions. Recent functional imaging in the infant ferret (Chapman & Bonhoeffer, 1994) has shown that responses to vertical and horizontal stimuli become apparent during postnatal development of V1 before responses to other orientations, as has earlier been reported for single unit responses in the kitten (Fregnac & Imbert, 1978). Newborn monkeys and those reared without visual experience also show a strong bias to horizontal and vertical orientation specificities (C. Blakemore & F. Vital Durand, personal communication). These findings suggest that orientation specificity is first built to orthogonal axes favouring vertical and horizontal in the visual field and it may be from these axes that other orientations are derived by interpolation. Recording in layer 4C of the adult macaque has shown orientation tuning to all orientations occurs in neurons at the top of layer 4C alpha, only occasional neurons turned to orientation in the middle of layer 4C and few orientation specific neurons in lower 4C (Hawken & Parker, 1984; Livingstone & Hubel, 1984); this appears to be confirmed by 2-deoxyglucose experiments showing regions of high and low activity in layer 4C alpha but uniform label in layer 4C beta after stimulation with oriented lines (Humphrey & Hendrickson, 1983; Tootell et al. 1988).

We suggest that a perfect retinotopic map found in recordings from nonoriented neurons in layer 4C of macaque V1 (Blasdel & Fitzpatrick, 1984) is all that is derived from the heavily overlapped thalamocortical afferents. The demonstration of laterally stepping axon connections of spiny stellate neurons making a single 300–500 μm step to one or both sides of a small extracellular injection of biocytin in mid layer 4C (Yoshioka et al. 1994*b*), as well as single spiny stellate cells intracellularly filled by micropipette showing lateral axon projections of similar morphology (Anderson et al. 1993) provides information regarding a possible substrate for initiating orientation specificity. While our extracelluar injections of biocytin in midlayer 4C all also showed a rising axon projection to layer 3B interblob positions, the intracellular filling of Anderson et al. suggests that the lateral sidestepping axons arise from spiny stellate neurons that do not project out of the layer; conversely, the spiny stellate neurons projecting out of the layer do not appear to provide laterally sidestepping axons. Finally, from our extracellular biocytin injections, it appears that the rising axon projections arise from all points across the mid 4C layer whereas the lateral sidesteps are less frequently observed. These single sidesteps are characteristic of midlayer 4C; in upper layer 4C alpha lateral connections are very much more extensive and in comparison to similar connections in the superficial layers (see later) they may link neurons of common orientation specificity.

Figure 7 illustrates our prediction, based on the anatomical data described above, for 3 types of spiny stellate neuron within layer 4C, all of which receive direct LGN input; type 1 neuron axons make only lateral projections in the layer and these terminate on type 2 neurons; type 2 neurons make projections out of the layer to layer 3B (to interblob regions; see Yoshioka et al. 1994*b*) and also locally to upper layer 4C alpha; type 2 neurons receive input from type 1 neurons as well as thalamic inputs; type 3 neurons

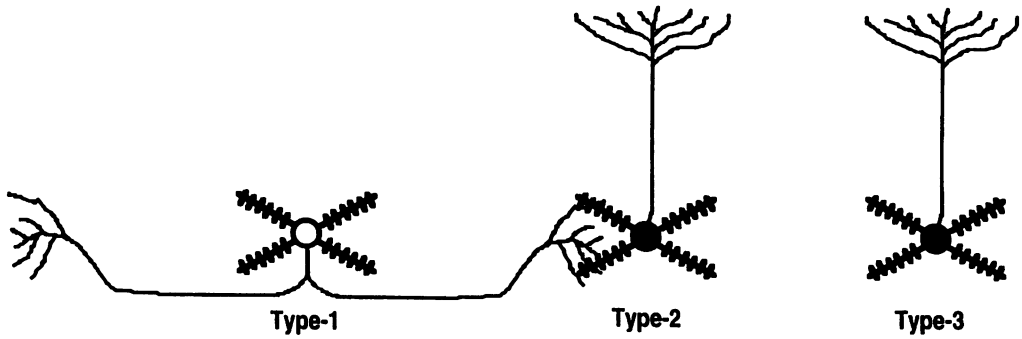

Fig. 7. Diagram of the 3 types of spiny stellate neuron suggested to populate midlayer 4C. Type 1 neurons provide only laterally sidestepping connections within mid layer 4C; type 2 neurons receive lateral projections from type 1 neurons and project vertically to layer 3b interblob regions; type 3 neurons provide vertical projections to layer 3 interblob regions but do not receive input from type 1 neurons. All these spiny stellate neurons receive input from thalamic afferents and all provide axon collaterals to their local environment.

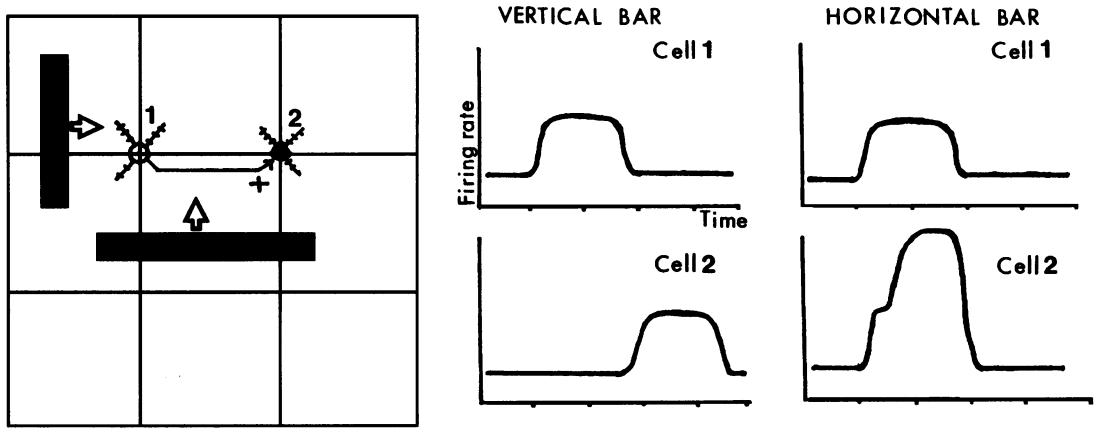

Fig. 8. Diagram illustrating the circuitry proposed for generating enhanced response to specific orientations of line stimuli. The vertically oriented bar stimulates cell 1 and cell 2 sequentially and under this condition both cells are driven equally well; if, instead, a horizontal bar crosses the visual fields of cell 1 and cell 2 simultaneously, the response of cell 2 is enhanced. A similar strategy could be employed for generating enhanced responses to vertical line orientation in a 2nd set of neurons.

project out of the layer to 3B and upper layer 4C but do not receive lateral projections from type 1 cells.

The effect of a type 1 spiny stellate sidestep is illustrated in Figure 8. In this diagram, a single horizontal type 1 sidestep to a type 2 neuron is depicted. A horizontal bar stimulus moving vertically across this arrangement of type 1 and 2 spiny stellate neurons activates the type 1 and type 2 neurons simultaneously. The response of the type 2 neuron, after a brief delay as the type 1 activity traverses the sidestep, is thus enhanced by the transferred activity from the concurrently stimulated type 1 cell. On the other hand, when a vertical bar stimulus moves in a horizontal direction from left to right over this geometry, the type 1 cell is activated first followed by the type 2 cell so that, because these cells are not jointly active, no enhancement to the type 2 cell activity occurs. So it follows that the type 2 neuron's response is optimal for horizontal stimuli. In an analogous fashion, replacing the horizontal sidestep with a type 1 sidestep to a vertically offset type 2 neuron instead, would render the target type 2 neuron's response optimal to vertical stimuli moving in a horizontal direction. Consequently the geometry of the type 1 neuron sidesteps can be used to form the basis of type 2 neuron orientation tuning patterns.

We suggest that axon projections from type 1 cells to type 2 cells have a local orthogonal geometry within mid layer 4C; for the moment our model suggests that a local T-shaped projection pattern of type 1 neuron to type 2 neuron would be a particularly powerful configuration. This would generate orientation preference in the type 2 cells for orthogonal line orientations, the retinotopic location of the type 1 cells relative to the type 2 cells to which they connect then becomes built in to the type 2 cell receptive fields and the type 1 cell input augments the type 2 cell response as is diagrammed in Figure 9.

These lateral connections within layer 4C could develop in utero along orthogonal directions locally within the lamina in response to waves of synchronous activity crossing the retina; a refractory period

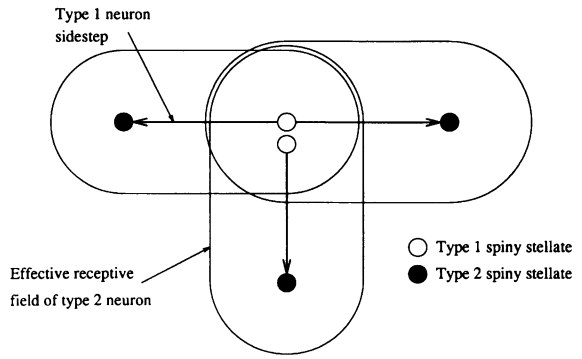

Fig. 9. T-shaped topographic map of type 1 spiny stellate neuron connections to type 2 spiny stellate neurons in layer 4C. Type 1 spiny stellate neurons are shown as open circles and type 2 as filled circles. The bar of the T arises from a bilateral type 1 neuron whilst the leg arises from a unilateral type 1 sidestep. The arrow shafts indicate the line orientation preference of each type 2 neuron while the arrowhead points to the position of the type 2 neuron receiving enhancing type 1 input. (Note particularly that the arrows do not indicate direction specificity). The distance from the cell body of each type 1 neuron to the type 2 cells to which it connects is approximately 350–600 μm. The blank space is filled by type 3 cells (see Fig. 8 for definition of the 3 cell types). Because type 2 cells, which have their own receptive fields, also receive type 1 inputs, the resultant type 2 receptive fields are effectively a combination of the type 2 and type 1 receptive fields elongated in the direction of the type 1 cell location as shown.

observed in embryonic retinal neurons which have just responded in synchrony to such travelling wave fronts may encourage orthogonal patterns of connectivity (Wong et al. 1993). The initial map of the retina within layer 4C begins as a binocular map but later becomes monocular as thalamic axons segregate into ocular dominance bands in layer 4C mainly during postnatal maturation (LeVay et al. 1980).

An economic mosaic of type 1 to type 2 spiny stellate cell connections within layer 4C could be built during development within midlayer 4C (a variety of orthogonal angles of orientation could be represented, but perhaps with emphasis on connections alternating along vertical and horizontal axes since these axes appear to dominate in the developing and mature states). The retinotopic map would continue to be represented point by point without orientation bias by type 3 spiny stellate neurons which we hypothesise to project to upper layer 4C and to layer 3B, like the type 2 neurons.

The 2nd step in our model of generation of orientation specificity involves generation of a full range of orientation specificities using the orthogonally tuned neuron population in midlayer 4C as start points. The type 2 mid 4C neurons provide local axon collaterals to upper layer 4 as well as sending rising axon projections to layer 3B and these type 2 axon fields would form a nonoverlapping mosaic in both regions given the proposed lateral separation of orthogonally oriented type 2 neurons in layer 4C and the spread of their rising axon fields (around 350 μm). In layer 3B (see Fig. 10) there is a close match between the lateral spread of single type 2 axon fields and the dendritic arbor spread of single layer 3B pyramidal neuron dendritic fields upon which they synapse (Lund & Yoshioka, 1991). Since pyramidal neuron dendritic fields are heavily overlapped in layer 3B, we predict that most pyramids will get input from both of the local orthogonally tuned type 2 layer 4C inputs as well as from the nonoriented type 3 neurons. A linear combination of these orthogonal orientation tuned inputs and the retinotopic type 3 inputs implemented as a feed-forward network, can generate orientations at interpolated angles in an orderly spatial gradient across the array of overlapped layer 3B pyramidal neurons (Hadingham & Lund, 1995).

The behaviour of the model for the T-shaped arrangement of type 1 and 2 spiny stellate neurons described above is depicted in Figure 11. The 4 vertical columns, for the stimulus orientations (from horizontal) of 0°, 45°, 90° and 135°, each comprise 3 plots generated by the model which is implemented in Mathematica (Wolfram, 1992). For each orientation the upper plot is the stimulus together with the responding type 2 cells, the middle contour plot the response of model upper layer 4C alpha and layer 3B neurons to this stimulus as a function of location (where light areas code for higher activity), and the lower graph the orientation dependence of the upper layer 4C alpha or layer 3B neuron which responds maximally to the orientation of the stimulus in the upper plot. Focusing on the middle row of plots, it is evident that the location of peak activity moves around the 'origin' of the T, i.e. where the type 1 cells are located, as the stimulus rotates around this origin. It is also clear that the activity of upper layer 4C alpha and layer 3B model neurons is broadly tuned to orientation (these same regions contain orientation specific neurons in the live animal; Hawken & Parker, 1984)) and this is confirmed in the lower row of graphs. Locations of peak activity are different for each orientation and this lower row of graphs represents the model orientation tuning of upper layer 4C alpha and layer 3B cells at the peak response location for each orientation. Note that the responses shown in the lower row represent the level of type 2 activity only at the respective points with the vertical scale in each case being the same. Cells at locations responding maximally to oblique orientations (2nd and 4th columns), in particular, are very broadly tuned.

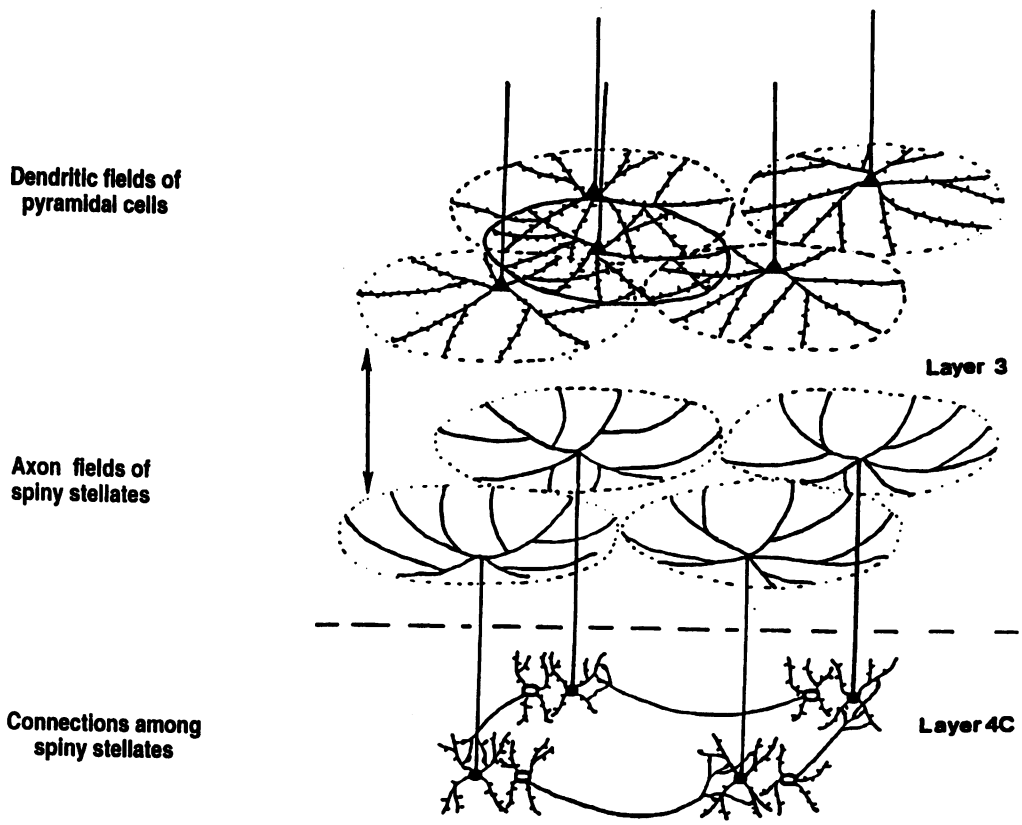

Fig. 10. Diagram illustrating projections of type 2 spiny stellate neurons in midlayer 4C to pyramidal neurons in layer 3B. There is a close match in scale between the diameter of the rising axon arbors and the spread of single pyramidal neuron dendritic fields (250–350 μm). While only 5 layer 3 pyramids are shown, there are in fact many closely packed pyramidal neurons with heavily overlapped dendrites (see text for further discussion).

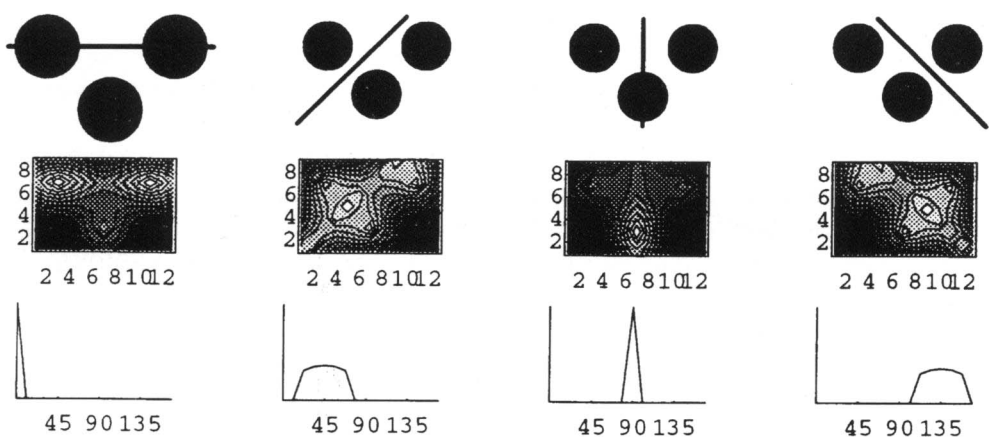

Fig. 11. Model responses to oriented stimuli. Each column of 3 plots pertains to model responses to the stimulus at the orientation and position shown in the upper plot. The filled circles in each upper plot show the relationship of type 2 cells to the respective stimulus. Contour plots in the middle row depict the pattern of activity of upper 4C alpha or layer 3B cells generated by each stimulus (lighter areas denote higher levels of activity). The retinotopic mapping of the stimulus in upper layer 4C alpha or layer 3B is evident from the contour patterns whose peaks rotate with the stimulus. It is clear that oblique stimuli (2nd and 4th columns) result in a broader spread of activity than that generated by horizontal or vertical stimuli. This is further illustrated in the lower row of graphs which shows model cell responses, each to the same scale (vertical axes), as a function of stimulus orientation (horizontal axes). In each case the model cell which gives the peak response to the given stimulus orientation is used to generate the plot; for example, the model cell at location (3, 5) is used for the 1st plot (horizontal stimulus) and the cell at (5,5) for the 2nd plot (45° oblique). Note that the effect of type 2 cell activity only is shown in this lower row of plots in order to highlight the orientation biasing this simulation provides. The relatively coarse resolution of this simulation is reflected by the axis labels in the middle row of the contour plots which shows a 12×8 grid of layer 3 cells was used.

To see how this continuous change in the location of peak response in upper layer 4C alpha and layer 3B neurons around the 'origin' of the T arises, consider Figure 12. Locations of peak response in these layers to horizontal and vertical stimuli are those directly overlying the type 2 neurons (see Fig. 10). Cell

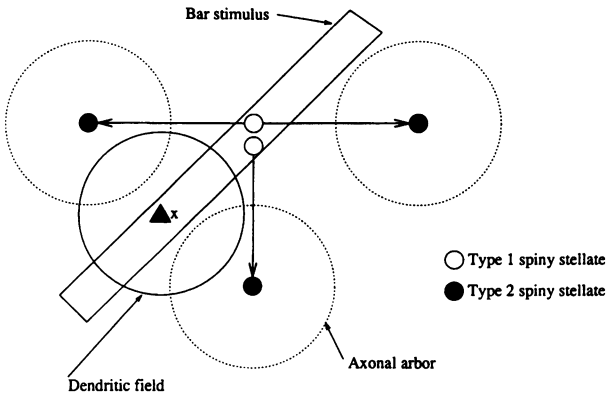

Fig. 12. Diagram showing how the orientation specificity of pyramidal neurons in layer 3 is generated from their dendritic overlap into spatially offset axon fields of layer 4C type 2 spiny stellate neurons with orientation preferences tuned to vertical and horizontal orientations (see text and previous figures). The full circle represents the position of the dendritic field of a layer 3 pyramidal neuron (×) overlaid on a local set of spatially offset, orthogonally tuned axon arbors (dotted circles) rising from layer 4C type 2 spiny stellate neurons. The oblique bar stimulus illustrated activates the type 1 spiny stellate neurons in this geometry which, in turn, activate their offset type 2 neurons which project their activity to layer 3 (see text for further details).

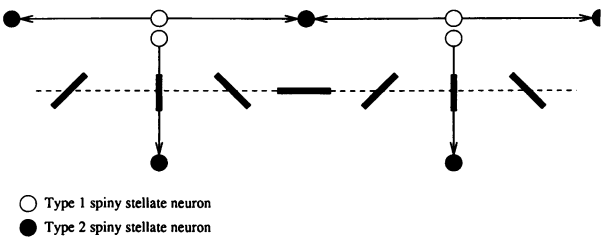

Fig. 13. Continuous changes in orientation could be generated by model 2 (see text and Figs 7–12) if a sequence of 2 T-shaped units are arranged as shown. Smooth orientation changes occur along the linear axis (shown dashed).

locations in these layers with peak responses to intermediate orientations receive input from more than one type 2 neuron, for example, the cell at location labelled 'x' in the figure. The dendritic field of this neuron overlaps the axonal arbors of 2 type 2 neurons. When an oblique bar stimulus simultaneously activates the neuron at 'x' and the type 1 neurons at the top of the leg of the T as illustrated in Figure 12, the activity of the 3 type 2 neurons at the extremities of the T is enhanced. Because of the overlap of 2 of these type 2 axonal arbors and the dendritic field of the upper layer 4C alpha or layer 3B neuron at 'x', the activity of this neuron is enhanced. After including the retinotopic type 3 input at this location (not shown in Fig. 12), the response of this cell is maximal for this oblique stimulus since a bar stimulus crossing the location 'x' at any other orientation will not maximally activate the type 1 cells with a consequent reduction of the type 2 enhancement. Similar arguments apply to other oblique orientations so that there is a continuous change in orientation preference around a polar axis with its origin at the mid point of the crossbar of the T.

In assessing these model results, it is pertinent to consider that what is being modelled is the response to total *excitatory* input to upper layer 4C alpha and 3B; no inhibitory effects have yet been considered. Additionally, the model is linear with a constant weight distribution which has the same value in each layer (see Hadingham & Lund, 1995 for details). Even so, a definite orientation bias in upper layer 4C and layer 3B cell response is discernible and this bias could be harnessed by neural circuitry designed to sharpen orientation tuning in these upper layers, such as that described by Somers et al. (1995) in their model of sharpening of orientation tuning of cortical neurons by recurrent local cortical excitation.

The linear map of orientation specificities generated across the cortical surface from our model (Fig. 11) can be constructed to be of the correct anatomical scale (i.e. to go from vertical to horizontal orientation and back to vertical preference takes approximately 600 μm, the width of 2 pyramidal neuron dendritic arbors). This is exemplified by the layout given in Figure 13 where the effect of linking a pair of T units horizontally is depicted. The dashed line in this figure provides a linear axis along which orientation preferences rotate continuously over a distance of more than 1 mm.

Further investigations of layout patterns of orthogonal T shaped units will be required in order to assess whether features detected in functional imaging experiments in vivo, such as saddle point singularities where orientation rotates through 180°, negative singularities of Y form and regions of slow orientation change (Blasdel & Salama, 1986; Malach et al. 1993; Obermayer & Blasdel, 1993) can be generated by the proposed interpolation model. As the ocular dominance stripes segregate out in layer 4C visual space becomes replicated for right and left eyes; we would predict that if our layer 4C template is distorted by field replication across the junction of the right and left eye domains, this will yield short stripelike iso-orientation domains in our model layer 3B, orthogonal to the ocular dominance bands as is seen in vivo.

Our model suggests that the layer 4C spiny stellate neurons that are tuned to 2 orthogonal orientations could, by their rising local axon collaterals in layer 4C, generate the full orientation gradients found in neurons of upper layer 4C alpha as well as the

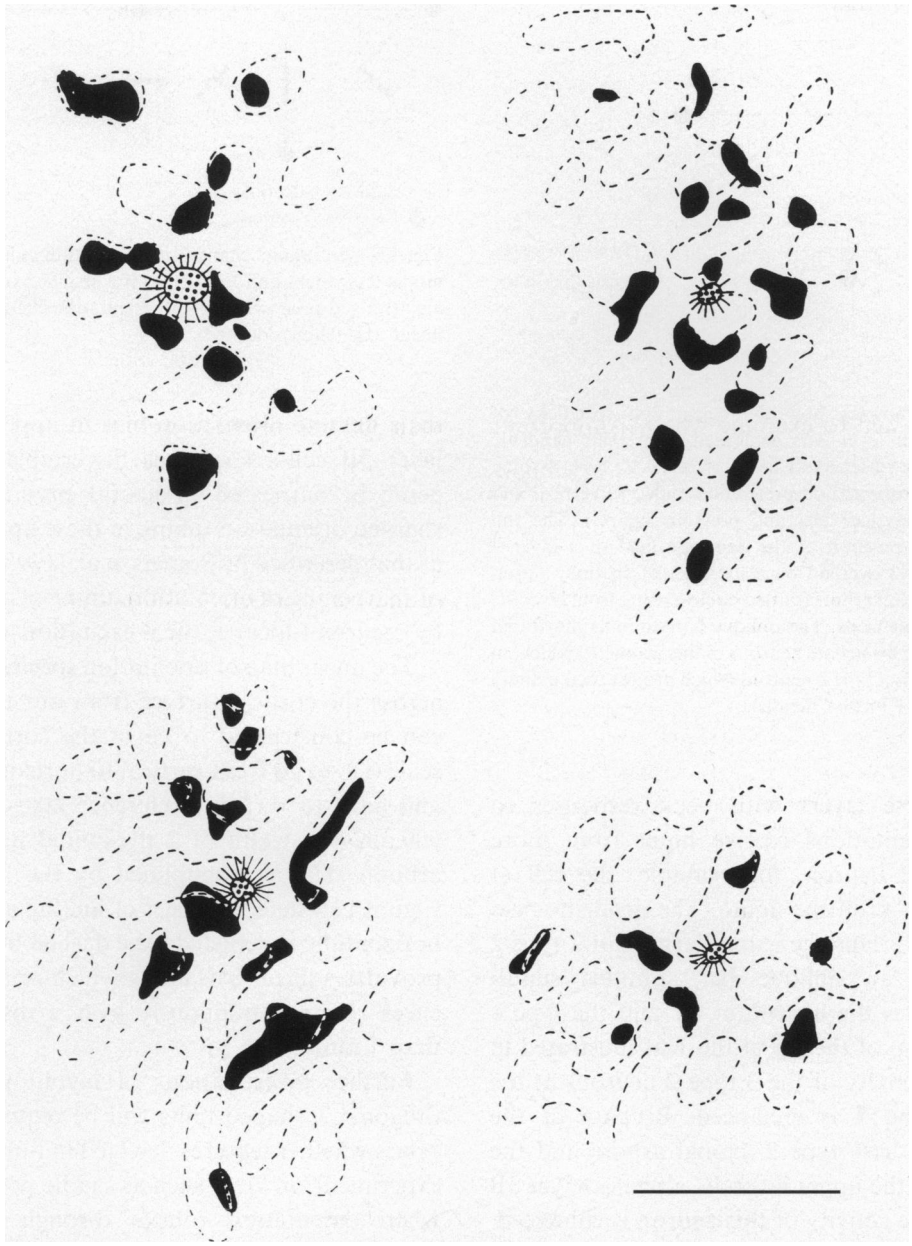

Fig. 14. Map of labelled axon terminal zones (black) arising from small iontophoretic injections of biocytin (fringed stippled circles) made into layers 2–3 of macaque V1. The positions of cytochrome oxidase rich terminal zones are enclosed by broken line parameters. Bar, 1 mm. (From Lund et al. 1993, by permission.)

gradients seen in layers 2 and 3. By overlaying separate systems carrying either ON or OFF signals in the initial orthogonal connectivity in layer 4C and establishing a mutual inhibition between ON and OFF fields at the same retinal locus (observed by Schiller, 1982), a basis for the parcellated fields of simple cells could be generated by convergence of spatially offset but similarly oriented cells to common layer 3B or upper 4C neurons.

In regard to the columnar representation of orientation specificity, where the same orientation is known to remain dominant in neurons recorded in vertical penetrations through cortical depth (Hubel & Wiesel, 1977) the anatomical circuitry of interlaminar projections (Blasdel et al. 1985; Fitzpatrick et al. 1985) shows that the major input to layer 5 arises from vertically descending axons from pyramidal neurons in the superficial layers; it would therefore appear that the topography of orientation specificity is mapped directly from superficial layers to layer 5 in strict alignment with the superficial layers. Layer 6 pyramidal neurons relate directly with layers 5, 4 and the superficial layers through vertically aligned apical dendritic arbors and recurrent axon relays; moreover, vertically descending projections from layer 4 excitatory and inhibitory neurons enter the neuropil of

layer 6 (Lund, 1987); it would seem plausible, therefore, that layer 6 neuron orientation specificities are also directly influenced by these interactions and the columnar alignment of orientation specificities through cortical depth reflects these multiple columnar links.

This model for generation of orientation specificity is compatible with known physiological and anatomical data for V1. It is very economical in its anatomical wiring and requires very little in terms of specificity in cell to cell connections. Importantly the model is testable by anatomical and physiological experiments designed to examine whether important features of the model actually exist, e.g. the existence of layer 4C orthogonal connections and the physiological dominance of responses to orthogonal orientation specificities in the same mid 4C region.

MODEL 3: LATERAL INTERACTIONS BETWEEN RECEPTIVE FIELD AND SURROUND REGIONS FOUND IN SINGLE UNIT RECORDINGS IN V1

In the superficial layers of V1 it is known that lateral connections made by the axon collaterals of pyramidal neurons run in patchy, lattice-like patterns across the neuropil of layers 2–4B (Rockland & Lund, 1983; Lund et al. 1993); these connections are predominantly between points of similar function, e.g. matched in ocular dominance, or blob or nonblob zones, or points that match in orientation specificity (Malach et al. 1993; Yoshioka et al. 1995). Any single point is therefore connected to a set of points around it with gaps between as shown in the anatomical reconstructions in Figure 14.

Injections of the tracer substance biocytin into the neuropil of layers 2–4B, covering a point no wider than 300 μm; produce an overall oval field of patches of terminal label measuring up to 3.7 mm across in perifoveal V1 cortex with the longer axis oriented at 90° to the ocular dominance columns, therefore probably representing a circular region in visual space (Lund et al. 1993; Yoshioka et al. 1995). Biocytin injections into the superficial layers, even if larger than a territory covering a repeat of all orientations, produce labelled patches of terminals that do not exceed the average diameter of a single pyramidal neuron dendritic field; the patches have a constant centre to centre distance and with terminal sparse

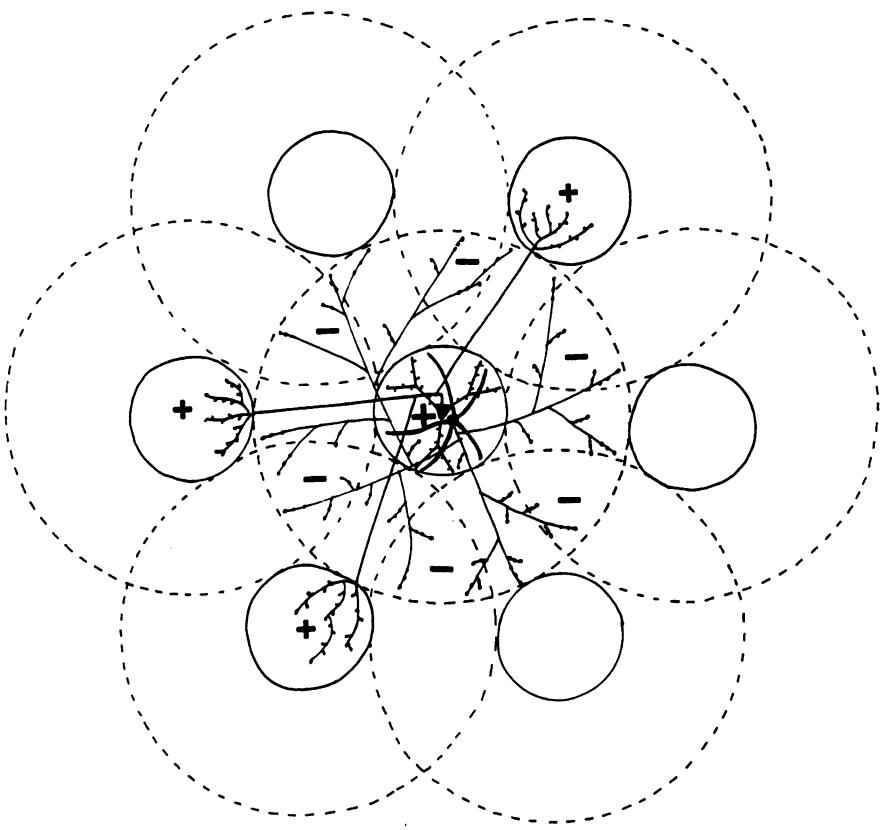

Fig. 15. Diagram of lateral connectivity of a single pyramidal neuron within the superficial layers of V1 together with the GABAergic (and presumed inhibitory) axon arbor distribution of a colocalised basket neuron. Coactivation of the pyramidal neuron and basket neuron would lead to a zone of inhibition around the pyramidal neuron covering regions of function unlike that of the pyramidal cell or its projection zones (from Lund et al. 1993, by permission). Small circles, patches of interconnected pyramids; large broken circles, axon fields of colocalised basket neurons.

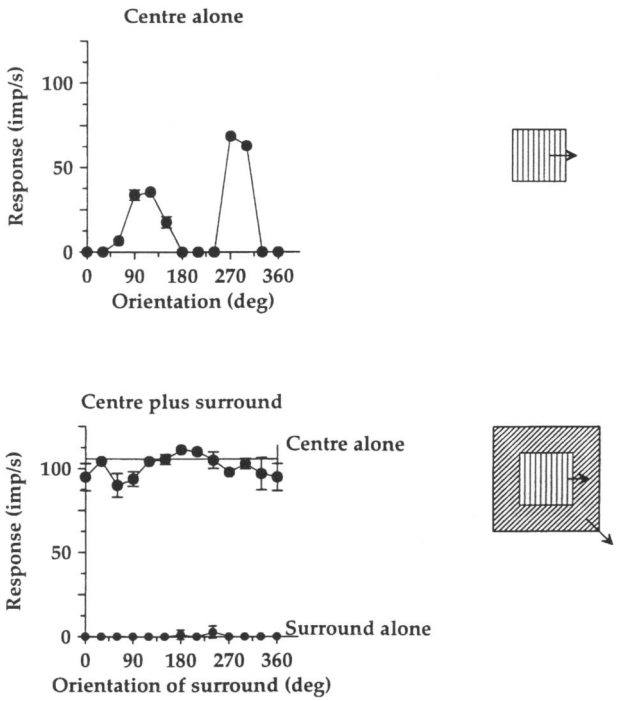

Fig. 16. Single unit data obtained from area V1 of paralysed, opiate anaesthetised macaque monkey, using drifting sinusoidal grating stimuli of the optimal spatial and temporal frequencies. The upper panel illustrates the orientation specific response of a layer of 6 complex cell elicited by stimulating its classical receptive field alone. This response is quite unaffected by concurrent stimulation of the surrounding field by lines of any orientation (below). In the situation shown in the lower panel the orientation of the centre stimulus is fixed at the optimal value for centre stimulation alone, and the orientation of stimuli in the surround is allowed to vary. The solid horizontal line (centre alone) represents the response to the optimal stimulus confined to the centre classical receptive field and the other data points indicate responses to the centre stimulus in the presence of surround stimuli of various orientations. It can be seen that response to the centre field optimal stimulus is virtually unchanged by surround stimulation.

gaps between them of the same diameter as the fully labelled terminal patches (Lund et al. 1993). If the biocytin injection is smaller in lateral extent than a single pyramidal neuron dendritic field it labels laterally spreading connections that terminate in patches smaller than a single pyramidal neuron dendritic field but still the same centre to centre spacing as with the fully labelled patches. It has been shown that the majority of synapses from the laterally spreading pyramidal neuron axons contact dendritic spines of other pyramidal neurons and in addition a small component contacts local circuit neuron dendritic shafts (Rockland, 1985; LeVay, 1988; McGuire et al. 1991). The pyramidal neuron axons are known to be excitatory to other pyramids and to GABAergic interneurons. Apart from the basket neurons, most local circuit neurons in the superficial layers have axon fields no larger than the dendritic field of local pyramidal neurons (e.g. chandelier neurons, cells with local beaded axons, cells with columnar axons; Lund & Yoshioka, 1991), and sometimes narrower (e.g. double bouquet cells). It has recently been shown that these patchy connections are already evident by E140 days in utero (Coogan & Van Essen, 1994; Yoshioka, 1994). Figure 15 illustrates this topography and shows that an inhibitory zone around each connected patch provided by basket neuron axons (which have an appropriate scale in vivo) could help create this system of patchy connections (Yoshioka et al. 1993). These basket neurons have a dendritic field that has the same lateral spread as that of the pyramidal neurons but whose axon reaches a total of 3 pyramidal neuron dendritic field widths, i.e. just wide enough for activity at any one point in the superficial layers to inhibit a surround zone of unlike properties, e.g. opposite orientation specificity.

Extracellular single unit physiological recording shows most individual neurons in area V1 to have a clearly defined 'classical' visual receptive field within which stimuli of particular properties, e.g. a particular line orientation, will elicite a brisk response from the cell. If stimuli are offered only outside the receptive field no response can be recorded. However, cells differ greatly in how their response to an optimal stimulus in their classical receptive field may be modified by simultaneously stimulating both the classical receptive field and the surround region (see e.g. Knierem & Van Essen, 1992). Data obtained from our own (Levitt & Lund, 1994) ongoing physiological studies of centre-surround interactions in macaque V1, shown in Figure 16 (upper) illustrate the orientation specific response, elicited by stimulating its classical receptive field alone, of a layer 6 complex cell from anaesthetised macaque V1 (see Figure legend for further details). This response is quite unaffected by concurrent stimulation of the surrounding field by lines of either the same or different orientation from those optimally driving the classic receptive field (Fig. 16, lower). In contrast, Figure 17 (upper) shows the response of a layer 4B cell to stimulate of its classical receptive field, which demonstrates that the cell is both orientation and direction specific, and Figure 17 (lower) illustrates that, in contrast to the layer 6 cell, there is marked inhibition of the cell's response to its preferred stimulus when the surround stimulus had the same configuration as the stimulus presented to the cell's classical receptive field. It is also observable that when the firing rate of the cell to preferred stimuli within its classical receptive field is weakened by reducing the contrast of the stimulus to the centre field, actual enhancement of its response to that stimulus is seen if the surround is stimulated by lines

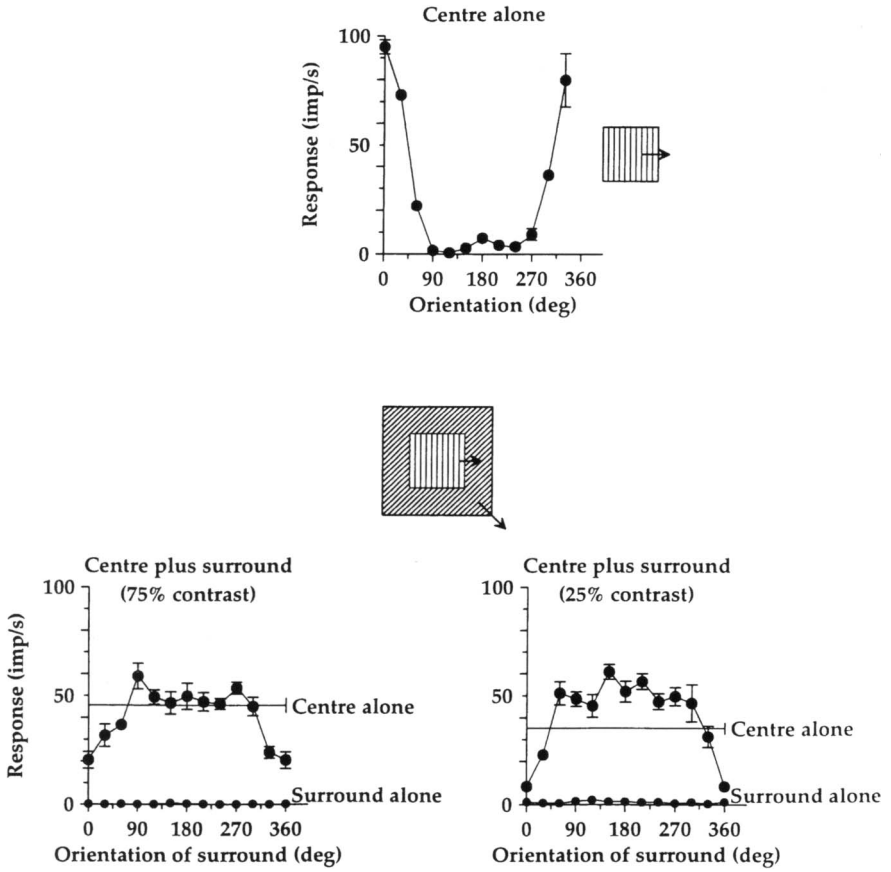

Fig. 17. Preparation as for Figure 16. Upper panel: response of a layer 4B complex cell to stimulation of its classical receptive field alone; the neuron is both orientation and direction specific. Lower panel: concurrent visual stimulation of central classical receptive field and surround stimulation by gratings of either the same or different orientation from those presented to the centre field. There is no response to surround stimulation alone. Left: both centre and surround at 75% contrast. Right: centre at 25% contrast, surround at 75% contrast). There is marked inhibition of the response to centre stimulation when surround orientation matches that in the centre; enhancement of the response to the centre by lines of nonmatching orientation in the surround can be seen when contrast at the centre is reduced to 25%.

differing in orientation from that used to drive the classical receptive field.

This modulation, by surround stimulation, of the response to stimulation of the classical receptive field, can take many different forms but we would like to suggest one anatomically based descriptive model (see Figs 18, 19) to explain the above interactions as an illustration of cortical modelling approaches.

Figure 18*A* presents a diagram of a single recorded pyramidal neuron (cell 1) whose preferred stimulus is an oblique bar as indicated above the neuron. This neuron is accompanied by a local inhibitory neuron (cell 2) whose axon arborises within the pyramidal neuron's dendritic field and contacts its dendrites. To one side is an offset pyramidal neuron (3) whose orientation preference is the same as the recorded neuron 1 and whose laterally running axon processes contact both neuron 1 and the local circuit neuron 2 (we know from in vivo studies that points of like orientation are interconnected in this fashion; T'so et al. 1986; Malach et al. 1993). Neuron 4 represents a pyramidal neuron and B, a basket neuron, which lie within territory maximally stimulated by lines of orthogonal orientation specificity to that preferred by neurons 1 and 3; therefore pyramidal neuron 4 will not connect to neurons 1 and 2, but the basket neuron lying with neurons of type 4 has an axon covering territory occupied by neuron 3. Figure 19 illustrates 2 conditions of stimulation of the receptive fields of pyramidal neurons 1 and 3, one (i) where only the classical receptive field of cell 1 is stimulated by its optimal orientation with minimal intrusion on the receptive fields of a set of neurons of type 3, and the other (ii) where the stimulus is extended so that bars of the same orientation cover the receptive field of the recorded neuron 1 as well as fully stimulating the receptive fields of the surrounding type 3 neurons of same orientation preference. Figure 18*B* maps the configuration of the input to pyramidal neuron 1 and to its inhibitory companion, cell 2: when only the classical receptive field of cell 1 is stimulated (stimulus condition (i) of Fig. 19) excitatory input to cells 1 and 2 from cells of type 3 is low and insufficient to affect the firing rates of cells 1 and 2; under stimulus

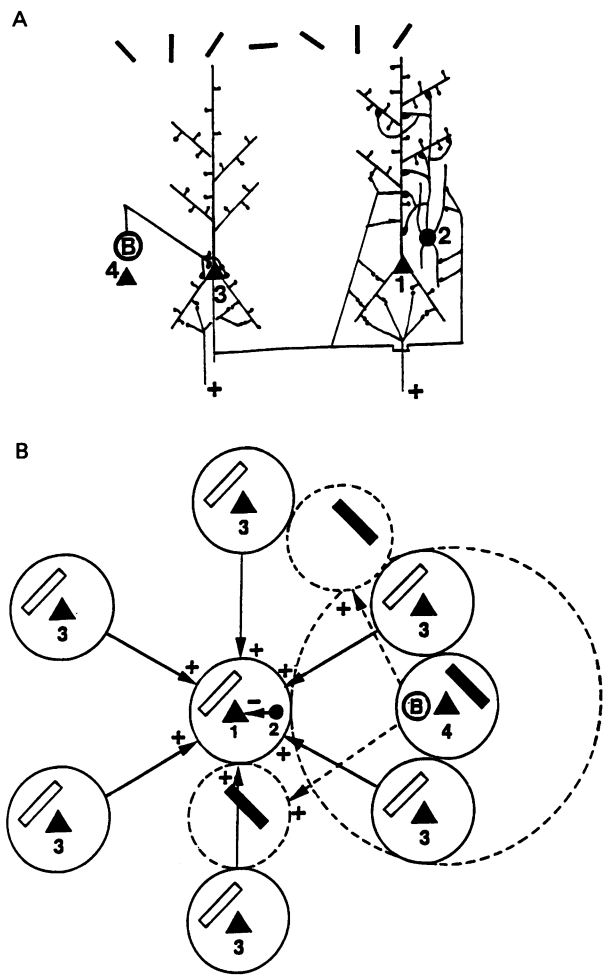

Fig. 18. Anatomical wiring used to explain centre-surround interactions described in the text and shown in Figure 17. (*A*) Two spatially offset layer 3 pyramidal neurons of similar orientation preference, cells 1 and 3, from area V1; cell 3 provides excitatory connections to cell 1 and to a local inhibitory neuron (cell 2) which synapses on cell 1. Pyramidal neuron 4, of opposite orientation preference to cells 1 and 3, is accompanied by an inhibitory basket neuron, B, whose excitatory inputs are the same as those driving cell 4 and whose axon contacts cell 3. (*B*) Tangential view of the same set of cells shown in (*A*), mapping the spatial topography of their dendritic fields (small circles) and axon connections (arrows). The large dotted ring indicates the axon field of basket neuron B. Small dotted circles indicate pyramidal neurons of same orientation preference as neuron 4 and its accompanying basket neuron B. Black oblique bars and open oblique bars indicate orientation preferences of cells occupying the small circles. In the text, 2 conditions of stimulation are described (illustrated in Fig. 19); in condition (i) only the classical receptive field of cell 1 is stimulated with little intrusion into the visual fields of cells of type 3. In (ii) the visual fields of cell 1 and cells of type 3 are stimulated concurrently by a large field of oriented bars (see text for further details).

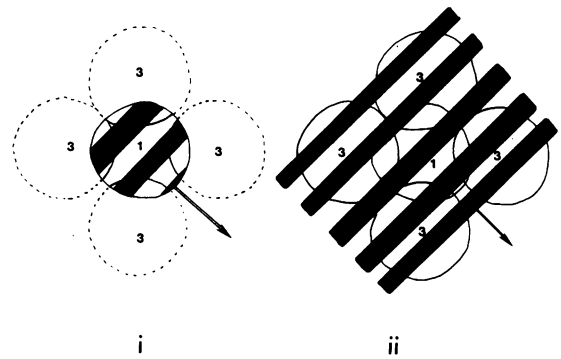

Fig. 19. Two conditions for visual field stimulation of neuron 1 and neurons of type 3 in Figure 18 (see text for model 3 for further explanation).

condition (ii) of Figure 19, where neurons of type 3 are now strongly activated, the weight of excitation to cells 1 and 2 rises and the inhibitory action of cell 2 on cell 1 begins to become strong enough to cause a decline in the response of cell 1, i.e. the net effect on neuron 1 is inhibition; the higher the activity rate of type 3 cells is compared with that of cell 1, the more weight of inhibition is exerted by cell 2 upon cell 1. As the orientation of the surround stimulus is changed, the activity of cells of type 3 will decline since the orientation is no longer optimal for them, and a spatially offset group of neurons tuned to the new orientation (cells like neuron 4 of Fig. 18) will become active; the group 4 pyramidal cells will not target the region occupied by cells 1 and 2 with their excitatory axons since they are of orthogonal orientation specificity; as inhibition from cell 2 on cell 1 declines with change of the surround line orientation away from that of the centre, the response of cell 1 to optimal stimulation of its classical receptive field returns. The relative contrast level (through its influence on firing rate) between centre and peripheral stimulus will also affect the precise position in the orientation gradient at which the surround switches from being inhibitory to facilitatory to cell 1; from Figure 17 it can be seen that when the centre is at 75% contrast compared with the surround, an angle of line in the periphery at 60° to that in the centre can be inhibitory, whereas the same angle is facilitatory when the centre contrast is only 25% that in the periphery. We suggest this is due to the different balance between direct excitation from layer 4C to neuron 1 through stimulation of its classical receptive field vs the interaction of local inhibition and excitation being driven on the same cell by lateral inputs within the more superficial layers from the surround under the 2 contrast conditions.

The movement of surround excitation to points of different orientation specificity from that of the recorded neuron 1 (such as neuron 4 of Fig. 18*B*) will elicit basket cell (B of Figure 18) activity in the surround territory that covers and inhibits the surround type 3 cell positions whose orientation matches that of the recorded neuron 1 (see Fig. 18*B*). This suppression of spontaneous activity of the type 3 neurons further reduces the excitation reaching cell 2

and in turn reduces its inhibition exerted on neuron 1, allowing enhancement of activity in a weakly active type 1 neuron (such as is induced by lowering the contrast of the stimulus on the classical receptive field; Fig. 17). This model predicts that when only the classical receptive field of cell 1 is stimulated, local inhibitory cell 2 is scarcely active (suggesting that the inhibitory cell 2 may not receive driving input from layer 4C afferents, unlike the pyramidal neurons). The inhibitory effect of the surround is quite tightly tuned for orientation in the neuron responses shown in Figure 17 and in fact becomes restricted to a territory representing only out to 45° from the orientation of the centre as the contrast in the centre is reduced, i.e. precisely that likely to be occupied by the dendritic field of pyramidal neuron 1. This suggests that the axon of the type 2 local circuit neuron is spatially restricted to that same territory and if it were recorded from when activated through its inputs from type 3 pyramidal neurons it should appear quite tightly orientation tuned (matched to the orientation of the type 3 pyramids) and show considerable spatial summation. The model further predicts that the wide arbor basket cells should be driven by the 4C afferents and endowed with orientation specificity in the same fashion as the local pyramids. The whole array of neurons just described should produce high activity at borders between regions of different pattern or contrast and lower activity within territory stimulated by constant pattern or luminance.

This descriptive model outlining a possible circuitry for at least one set of centre-surround effects seen in physiological recording in V1 utilises real features of anatomical circuitry observed in area V1 and is testable using anatomical and physiological methods in the real animal. It is particularly interesting to the cortical anatomist in that it predicts possible roles for some of the observed forms of local circuit GABAergic neurons. Many other forms of centre surround interactions are observed and it is probable that they differ between laminae. We are currently exploring this possibility in our ongoing physiological studies.

SUMMARY

We have used known features of area V1 anatomy and physiology to construct three simple models to explain important features of the functional activity of the region. While we hope these models are accurate reflections of the organisation of the real cortex, we shall be particularly pleased if they are sufficiently interesting enough to spur others to test their validity by means of further biological experiments; in testing the predictions of the models we will undoubtably learn more about the organisation of the region and this will be sufficient reward even if some aspects of these particular models are proven inaccurate.

We are confident that since many regions of cortex share a common, lattice-like intraareal connectional architecture and that gradients of function repeat at a common scale to these connections in each area, if models for one area prove correct, they should apply with only slight changes to other regions. It is worth therefore trying to make models as anatomically and physiologically realistic as possible and so make predictions that can be tested in the laboratory to verify, modify, or refute the particular model architecture.

ACKNOWLEDGEMENTS

This work was supported by NIH-NEI grant EY10021, MRC grants 9203679N and G9408137, and International Human Frontier Science Program RG-98/94B.

REFERENCES

ANDERSON JC, MARTIN KAC, WHITTERIDGE D (1993) Form, function and intracortical projections of neurons in the striate cortex of the monkey *Macacus nemestrinus*. *Cerebral Cortex* **3**, 412–420.

BLAKEMORE CB, GAREY LJ, VITAL-DURAND F (1981) Orientation preferences in the monkey's visual cortex. *Journal of Physiology (London)* **309**, 78P.

BLASDEL GG, FITZPATRICK D (1984) Physiological organization of layer 4 in macaque striate cortex. *Journal of Neuroscience* **12**, 3141–3163.

BLASDEL GG, LUND JS (1983) Termination of afferent axons in macaque striate cortex. *Journal of Neuroscience* **3**, 1389–1413.

BLASDEL GG, LUND JS, FITZPATRICK D (1985) Intrinsic connections of macaque striate cortex: axonal projections of cells outside lamina 4C *Journal of Neuroscience* **5**, 3350–3369.

BLASDEL GG, SALAMA G (1986) Voltage sensitive dyes reveal a modular organization in monkey striate cortex. *Nature* **321**, 579–585.

BULLIER J, HENRY GH (1980) Ordinal position and afferent input of neurons in monkey striate cortex. *Journal of Comparative Neurology* **193**, 913–935.

CHAPMAN B, ZAHS KR, STRYKER MP (1991) Relation of cortical cell orientation selectivity to alignment of receptive fields of the geniculocortical afferents that arborize within a single orientation column in ferret visual cortex. *Journal of Neuroscience* **11**, 1347–1358.

CHAPMAN B, BONHOEFFER T (1994) Chronic optical imaging of the development of orientation domains in ferret area 17. *Society for Neuroscience Abstracts* **20**, 214.

COOGAN TA, VAN ESSEN DC (1994) Early development of modular connections in V1 and V2 of macaque monkeys. *Society for Neuroscience Abstracts* **20**, 215.

DERRINGTON AM, LENNIE P (1984) Spatial and temporal contrast sensitivities of neurons in lateral geniculate nucleus of macaque. *Journal of Physiology (London)* **357**, 219–240.

FERSTER D, KOCH C (1987) Neuronal connections underlying orientation selectivity in cat visual cortex. *Trends in Neuroscience* **10**, 487–497.

FITZPATRICK D, LUND JS, BLASDEL GG (1985) Intrinsic connections of macaque striate cortex: afferent and efferent connections of lamina 4C. *Journal of Neuroscience* **5**, 3329–3349.

FREGNAC Y, IMBERT M (1978) Early development of visual cortical cells in normal and dark-reared kittens: relationship between orientation selectivity and ocular dominance. *Journal of Physiology (London)* **278**, 27–44.

HADINGHAM P, LUND JS (1995) A visual cortex circuit model for orientation specificity. *Proceedings of the Institution of Electrical and Electronic Engineers International Conference on Neural Networks*, Perth, Australia.

HAWKEN MJ, PARKER AJ (1984) Contrast sensitivity and orientation selectivity in lamina IV of the striate cortex of old world monkeys. *Experimental Brain Research* **54**, 367–372.

HICKS TP, LEE BB, VIDYASAGAR TR (1983) The responses of cells in the macaque lateral geniculate nucleus to sinusoidal gratings. *Journal of Physiology, (London)* **337**, 183–200.

HUBEL DH, WIESEL TN (1972) Laminar and columnar distribution of geniculocortical fibers in macaque monkey. *Journal of Comparative Neurology* **146**, 241–450.

HUBEL DH, WIESEL TN (1977) Receptive fields and functional architectures of monkey striate cortex. *Journal of Physiology (London)* **195**, 215–245.

HUMPHREY AL, HENDRICKSON AE (1983) Background and stimulus-induced patterns of high metabolic activity in the visual cortex (area 17) of the squirrel and macaque monkey. *Journal of Neuroscience* **3**, 345–358.

JENKINS B (1985) Orientational anisotropy in the human visual system. *Perception and Psychophysics* **37**, 125–134.

KISVÁRDAY ZF, COWEY A, SOMOGYI P (1986) Synaptic relationship of a type of GABA-immunoreactive neuron (clutch cell), spiny stellate cells and lateral geniculate nucleus afferents in layer IVC of the monkey striate cortex. *Neuroscience* **19**, 741–761.

KNIEREM JJ, VAN ESSEN DC (1992) Neuronal responses to static texture patterns in area V1 of the alert macaque monkey. *Journal of Neurophysiology* **67**, 961–980.

LEVAY S (1988) Patchy intrinsic connections in visual cortex, area 18, of the cat: morphological and immunocytochemical evidence for an excitatory function. *Journal of Comparative Neurology* **269**, 265–274.

LEVAY S, WIESEL TN, HUBEL DH (1980) The development of ocular dominance columns in normal and visually deprived monkeys. *Journal of Comparative Neurology* **191**, 1–51.

LEVITT JB, LUND JS (1994) Orientation and direction selective effects from beyond the classical receptive field in macaque striate and prestriate neurons. *Society for Neuroscience Abstracts* **20**, 428.

LIVINGSTONE MS, HUBEL DH (1984) Anatomy and physiology of a color system in the primate visual cortex. *Journal of Neuroscience* **4**, 309–356.

LUND JS (1987) Local circuit neurons of macaque monkey striate cortex: I. Neurons of laminae 4C and 5A. *Journal of Comparative Neurology* **247**, 455–496.

LUND JS (1990) Excitatory and inhibitory circuitry and laminar mapping strategies in primary visual cortex of the monkey. In *Signal and Sense: Local and Global Order in Perceptual Maps* (ed. G. M. Edelman, W. E. Gall & W. M. Cowan), pp. 51–66. New York: John Wiley and Sons.

LUND JS, HOLBACH S (1991) Postnatal development of thalamic recipient neurons in monkey striate cortex: I. A comparison of spine acquisition and dendritic growth of layer 4C α and β spiny stellate neurons. *Journal of Comparative Neurology* **309**, 115–128.

LUND JS, YOSHIOKA T (1991) Local circuit neurons of macaque monkey striate cortex: III. Neurons of laminae 4B, 4A, and 3B. *Journal of Comparative Neurology* **311**, 234–258.

LUND JS, YOSHIOKA T, LEVITT JB (1993) Comparison of intrinsic connectivity in different areas of macaque monkey cerebral cortex. *Cerebral Cortex* **3**, 148–162.

MALACH R, AMIR Y, HAREL M, GRINVALD A (1993) Relationship between intrinsic connections and functional architecture revealed by optical imaging and in vivo targeted biocytin injections in primate striate cortex. *Proceedings of the National Academy of Sciences of the USA* **90**, 10469–10473.

MATES SL, LUND JS (1983) Developmental changes in the relationship between type 2 synapses and spiny neurons in the monkey visual cortex. *Journal of Comparative Neurology* **221**, 98–105.

MCGUIRE BA, GILBERT CD, RIVLIN PK, WIESEL TN (1991) Targets of horizontal connections in macaque primary visual cortex. *Journal of Comparative Neurology* **305**, 370–392.

MAUNSELL JHR, GIBSON JR (1992) Visual response latencies in striate cortex of macaque monkey. *Journal of Neurophysiology* **68**, 1332–1344.

OBERMAYER K, BLASDEL GG (1993) Geometry of orientation and ocular dominance columns in monkey striate cortex. *Journal of Neuroscience* **13**, 4114–4129.

O'KUSKY JR, COLONNIER M (1982) Postnatal changes in the numbers of neurons and synapses in the visual cortex (area 17) of the macaque monkey; a stereological analysis in normal and monocularly deprived animals. *Journal of Comparative Neurology* **210**, 291–306.

PETERS A, PAYNE BR, BUDD J (1994) A numerical analysis of the geniculocortical input to striate cortex in the monkey. *Cerebral Cortex* **4**, 215–229.

POGGIO GF, FISCHER B (1977) Binocular interaction and depth sensitivity in striate and prestriate cortex of behaving rhesus monkey. *Journal of Neurophysiology* **40**, 1392–1405.

ROCKLAND KS, LUND JS (1983) Intrinsic laminar lattice connections in primate visual cortex. *Journal of Comparative Neurology* **216**, 303–318.

ROCKLAND KS (1985) Intrinsically projecting pyramidal neurons of monkey striate cortex: an EM-HRP study. *Society for Neuroscience Abstracts* **11**, 17.

SCHILLER PH (1982) Central connections of the retinal ON and OFF pathways. *Nature* **297**, 580–583.

SHAPLEY R (1990) Visual sensitivity and parallel retinocortical channels. *Annual Review of Psychology* **41**, 635–658.

SHAPLEY R, KAPLAN E, SOODAK R (1981) Spatial summation and contrast sensitivity of X and Y cells in the lateral geniculate nucleus of the macaque. *Nature* **292**, 543–545.

SOMERS DC, NELSON SB, SUR M (1995) An emergent model of orientation selectivity in cat visual cortical simple cells. *Journal of Neuroscience* **15**, 5448–5465.

TOOTELL RBH, HAMILTON SL, SWITKES E (1988) Functional anatomy of macaque striate cortex. IV. Contrast and magnoparov streams. *Journal of Neuroscience* **5**, 1594–1609.

T'SO DY, GILBERT CD, WIESEL TN (1986) Relationships between horizontal connections and functional architecture in cat striate cortex as revealed by cross correlation analysis. *Journal of Neuroscience* **6**, 1160–1170.

WIESEL TN, HUBEL DH (1966) Spatial and chromatic interactions in the lateral geniculate body of the rhesus monkey. *Journal of Neurophysiology* **29**, 1115–1156.

WOLFRAM S (1991) *Mathematica: A System for Doing Mathematics by Computer*, 2nd edn. New York: Addison-Wesley.

WOLFRAM S (1992) *Mathematica*. Champaign, IL: Wolfram Research .

WONG RO, MEISTER M, SHATZ CJ (1993) Transient period of correlated bursting activity during development of the mammalian retina. *Neuron* **11**, 923–938.

WU Q, LUND JS, LEVITT JB (1995) An anatomically based neural

network model of the circuitry within layer 4C of primary visual cortex in macaque. *Investigative Ophthalmology and Visual Science* (ARVO Suppl.) **35**, 1828.

YOSHIOKA T (1994) Development of clustered lateral connectivity in macaque visual cortex. *Society for Neuroscience Abstracts* **20**, 1109.

YOSHIOKA T, LEVITT JB, LUND JS (1994) Independence and merger of thalamocortical channels within macaque monkey primary visual cortex: anatomy of interlaminar projections. *Visual Neuroscience* **11**, 467–489.

YOSHIOKA T, BLASDEL GG, LEVITT JB, LUND JS (1995) Relation between patterns of intrinsic lateral connectivity, ocular dominance, and cytochrome oxidase-reactive regions in macaque monkey striate cortex. *Cerebral Cortex*, in press.